Chapter 6

Preliminary microphysical studies using the AMS

The role of aerosols in cloud formation and precipitation is increasingly acknowledged[1]. Such indirect climate effects due to aerosols have recently been cited as potentially matching the importance of the effects of greenhouse gases[2]. A critical quantity in this regard is the water uptake by an aerosol of a given composition and size. For simple systems such as oleic acid, we show how to measure Henry's law water solubility within the particle, including a preliminary experimental study of this system. We also consider water uptake on salts (for deliquescence or efflorescence studies) and for soot coated with sulfuric acid. Finally a preliminary study of submicron sulfuric acid microphysics is presented. In this study we demonstrate how to separate nucleation, condensation, and coagulation processes. Theoretical rate constants are derived, and a method is outlined for the experimental measurement of coagulation rates.

6.1 Water uptake studies

Because gas phase diffusion and solubility have very small characteristic times (see ch. 4), the AMS / Flowtube system described in ch. 5 can be used to study equilibrium phenomena such as deliquescence and efflorescence. In this case, one need only replace the reactive trace gas with water.

6.1.1 Deliquescence of salts

Studies of aerosol size change as a function of relative humidity using the AMS start with an understanding of expected shifts in aerodynamic diameter with composition. Here we derive a simple expression for aerodynamic diameter changes as a function of water mole fraction. We begin by developing an expression for the aerodynamic diameter of a particle with a known mass of salt and water. From the definition of the aerodynamic diameter (for detail, see ch. 3):

$$D_a \equiv s\beta D \tag{6.1}$$

Here s is the specific gravity of the particle and β is the particle shape factor. If a salt has begun to take up water, then we will assume it is a solution and thus spherical. It follows that the wet diameter reduces to sD, where D is the geometric diameter. We can write the specific gravity of the particle as:

$$s \equiv \frac{n_s M_s + n_w M_w}{\rho_w \pi D^3 / 6} \tag{6.2}$$

Here n_s and n_w represent the number of moles of salt and water in the particle, M_s and M_w are the molecular weights (g/mole) of the salt and of water, and ρ_w is the density of water (g/cc). If we make the assumption that the partial molar volumes of the components are constant (the density of each species is unchanged from its pure value), then the volume of the particle can be equated to the sum of the volumes of each component. Thus we have:

$$\frac{\pi D^3}{6} = \frac{M_s n_s}{\rho_s} + \frac{M_w n_w}{\rho_w} \tag{6.3}$$

Solving eq. 6.3 for D and multiplying by eq. 6.2 (having substituted 6.3 in the numerator) supplies us with an expression for the "wet" aerodynamic diameter:

$$D_a = sD = \frac{1}{\rho_w}\left(\frac{6}{\pi}\right)^{1/3}\left(\frac{n_w M_w}{\rho_w} + \frac{n_s M_s}{\rho_s}\right)^{-2/3}(n_s M_s + n_w M_w) \tag{6.4}$$

From the definition of the mole fraction, we can express n_w as a function of the mole fraction of water and the initial number of moles of the salt:

$$n_w = \frac{n_s x_w}{1 - x_w} = \frac{n_s x_w}{1 - x_w} = \frac{x_w}{1 - x_w}\frac{\rho_s}{M_s}V_o \tag{6.5}$$

In eq. 6.5, we have introduced V_0 as the initial volume of the dry salt, so we can combine it with 6.4 and write:

$$D_a(x_w, V_0) = \frac{1}{\rho_w}\left(\frac{6}{\pi}\right)^{1/3}\left(\frac{n_w(x_w, V_0)M_w}{\rho_w} + V_0\right)^{-2/3}(\rho_s V_0 + n_w(x_w, V_0)M_w) \tag{6.6}$$

For most salts of atmospheric interest, $\rho_s > \rho_w$ and as x_w increases, the specific gravity of the particle will decrease. This counters the effect of the geometric diameter, increasing with water uptake (assuming constant partial molar volumes as before). The net effect is that $D_a(x_w)$ will have a minimum at a certain critical x_w.

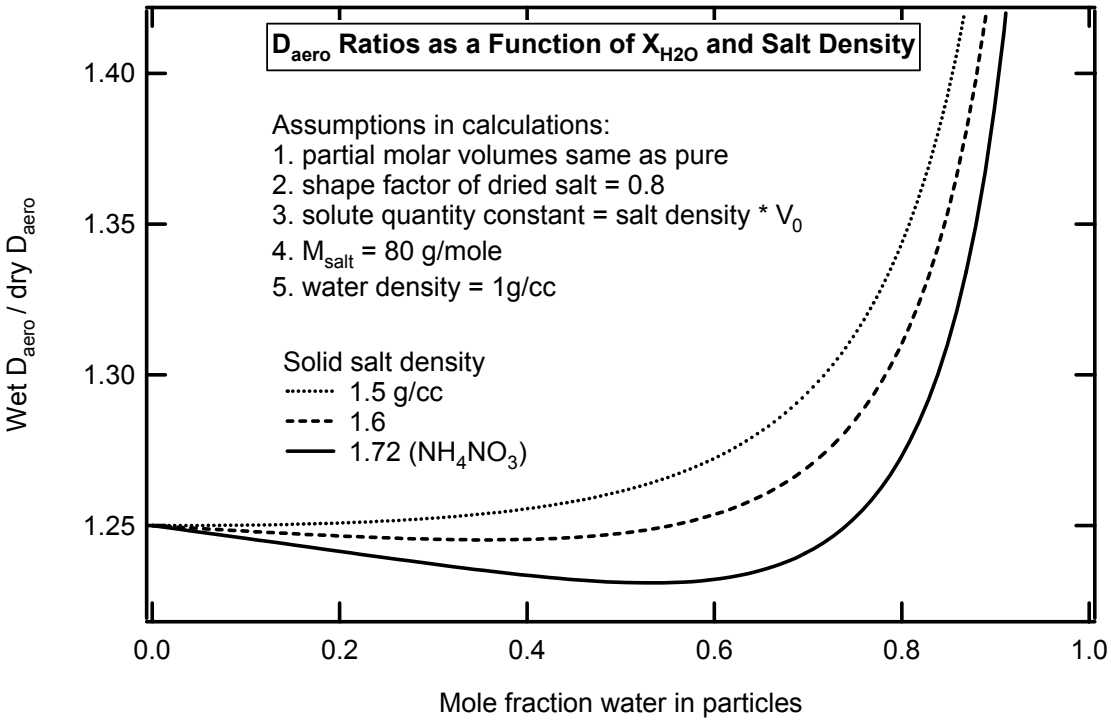

Figure 6-1: Increasing mole fraction of water tends to decrease the particle density while increasing the geometric diameter, such that the product (aerodynamic diameter) passes through a minimum.

In fig. 6-1, we plot eq. 6.6 (normalized to an initial dry D_a) showing how the minimum shifts with salt density. The plot does not show the most dramatic change, deliquescence, when the particle passes from solid to liquid and its shape factor changes abruptly.

6.1.2 Henry's law solubility of water in oleic acid

Equation 6.6 can be used to extract the mole fraction of water present in spherical particles whose initial volumes are known. This information can be supplemented with knowledge of the relative humidity to supply solubility information. In the case where the density change in the particles is negligible, one can obtain a simpler expression than eq. 6.6. From conservation of mass:

$$\frac{\rho\pi D^3}{6} = \frac{\rho\pi D_0{}^3}{6} + HP_xM_x\frac{\pi D^3}{6} \tag{6.7}$$

Here H (M atm^{-1}) is the Henry's law solubility of species x in the particle. With some rearrangement, we may simplify to:

$$H = \frac{1}{P_xM_x}\frac{D^3 - D_0{}^3}{D^3} = \frac{1}{P_xM_x}\frac{\Delta V}{V} = \frac{1}{P_xM_x}(1-(\frac{D}{D_0})^{-3}) \tag{6.8}$$

For the case where x = water, we can write this as a function of the relative humidity (0 to 1) by substituting: $P_x = P_w = RH\ P_w{}^o$. Eq. 6.8 therefore enables us to calculate Henry's law coefficients from the fractional volume change of the particles. Such information can be compared to mass spectra to provide complementary sources of information on physical uptake of trace gases.

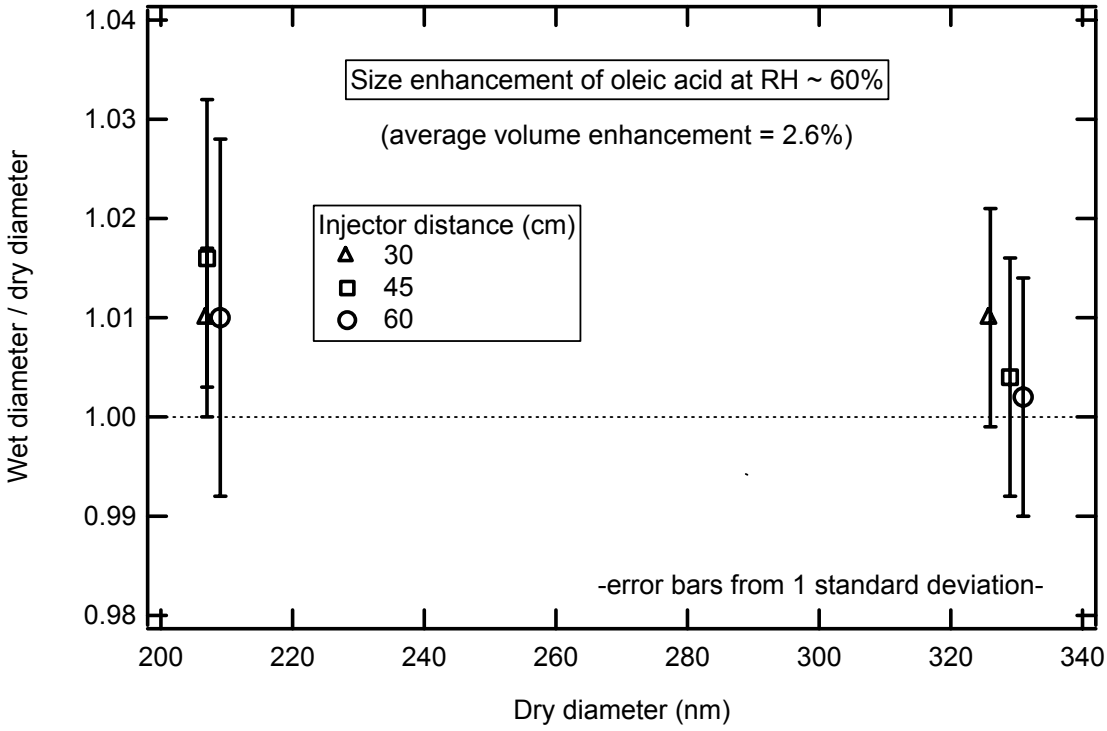

Figure 6-2: Aerodynamic diameter ratios used to calculate Henry's law equilibrium constant for water in oleic acid.

Figure 6-2 shows a plot of the aerodynamic diameter ratio (which in this case equals the geometric diameter ratio) in the presence of known RH for two sizes at three different injector distances (to verify equilibrium conditions). This preliminary data was used to estimate a Henry's law value for water in oleic acid of 70 M atm^{-1}.

6.1.3 Water uptake on sulfuric acid activated soot

The study of water uptake on sulfuric acid activated soot particles requires a slightly more complicated set-up than was used for water uptake on oleic acid, as it is necessary to coat the soot with sulfuric acid in a controllable fashion. This is achieved by warming the soot and its entrainment air, allowing it to flow into a sulfuric acid vapor reservoir of the same temperature, with the air newly saturated in sulfuric acid later cooled as it flows.

The entrainment air, now supersaturated in sulfuric acid, cools in such a way as to allow condensation on the soot aerosols. One must use care that there are enough soot particles per volume of air that homogeneous nucleation of the soot does not compete with condensation. The cooled and coated soot is then flowed into a similar flowtube apparatus as was described for the oleic acid/ozone experiment (ch. 5). The trace gas in this case is water. Ideally one uses both mass spectra and changes in aerodynamic diameter to study size change and water uptake as a function of aerosol size and sulfuric acid loading. In this preliminary presentation, we only show results for the size change with a focus on the method of analysis.

Using similar arguments as were used to derive eq. 6.6, one can show that the ratio of aerodynamic diameters for sulfuric acid activated soot at two different relative humidities is given by:

$$\frac{D_a}{D^o{}_a} = \left(\frac{\rho}{\rho_o}\right)^{2/3} \left(\frac{m_w + m_s{}^o + m_\sigma{}^o}{m_w{}^o + m_s{}^o + m_\sigma{}^o}\right)^{1/3} \tag{6.9}$$

This particular model assumes that sulfuric-acid-coated soot is spherical, and that water is absorbed only in the aqueous component of the particle. We also assume that the mass of soot, m_σ^o in the initial particle of size D_o is known. From the water / sulfuric acid equilibrium composition diagram (describing the mass fraction of water as a function of RH), we may take the initial mass of water $m_w{}^o$ to be used in eq. 6.9 as:

$$m_w{}^o(D_o, RH_0) = \frac{m_s{}^o(D_0)\, w(RH_0)}{1 - w(RH_0)} \tag{6.10}$$

Here, w is the mass (weight) fraction of water in the aqueous portion of the aerosols. Likewise the final mass of water present in the particle may be written as:

$$m_w(D_o, RH) = \frac{m_s{}^o(D_0)w(RH)}{1 - w(RH)} \tag{6.11}$$

In eq. 6.11 we note that the mass of water is still proportional to the original amount of sulfuric acid in the particles, as this quantity does not change upon addition of water vapor to the system. Introducing another quantity f_s, the fraction of the initial particle mass which is sulfuric acid, we may express the mass of sulfuric acid in the particles as:

$$m_s{}^o(D_o) = \frac{f_s(D_0)m_\sigma{}^o(D_0)}{1 - f_s(D_0)} \tag{6.12}$$

We may also develop expressions for the specific gravities (or densities in g/cc) used in eq. 6.9:

$$\rho_o = \frac{m_s{}^o + m_w{}^o + m_\sigma{}^o}{m_s{}^o(1 - f_s)(f_s\rho_\sigma)^{-1} + (m_w{}^o + m_s{}^o)(\rho_{aq}{}^0)^{-1}} \tag{6.13}$$

and

$$\rho = \frac{m_s{}^o + m_w + m_\sigma{}^o}{m_s{}^o(1 - f_s)(f_s\rho_\sigma)^{-1} + (m_w + m_s{}^o)(\rho_{aq})^{-1}} \tag{6.14}$$

In both these expressions, ρ_{aq} represents the equilibrium density of the sulfuric acid / water solution around the soot. It is represented as a given function of RH, taken from measurements or equilibrium calculations available in the literature.

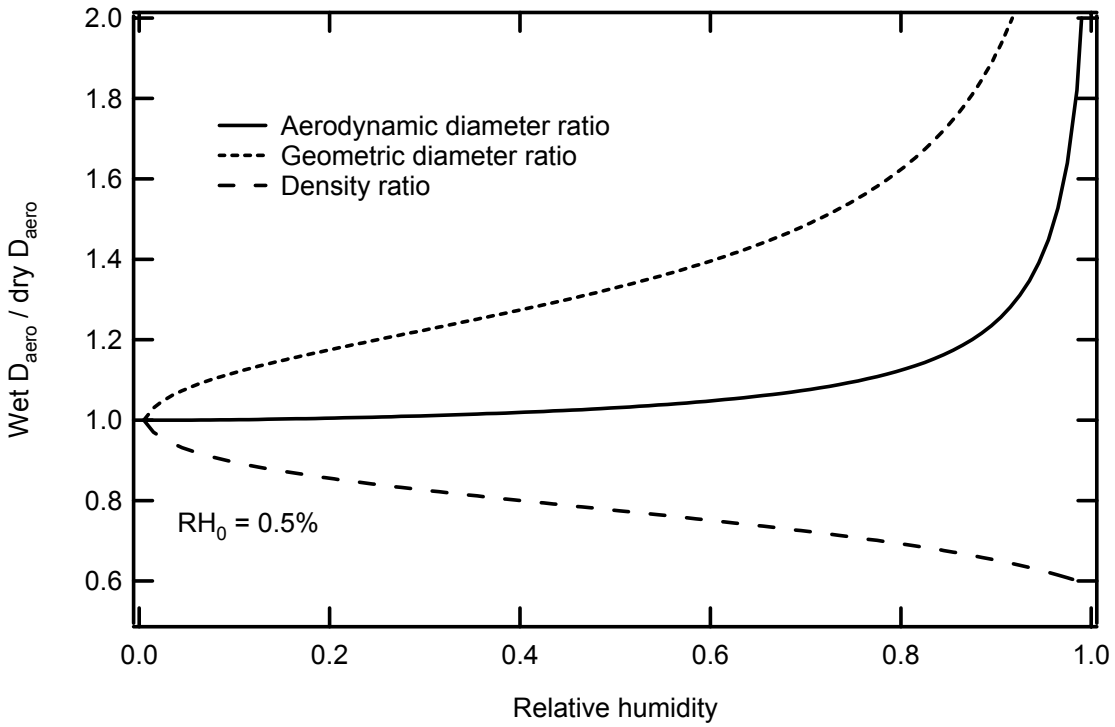

Figure 6-3: The functional dependence of sulfuric acid particle growth with relative humidity. Known equilibrium curves for the mole fraction of water in solution with sulfuric acid as a function of RH, and density as a function of mole fraction were used. The effects of density change and geometric diameter change tend to cancel such that significant growth is not expected below 50 % RH.

The density of the soot spherules ρ_σ (i.e. soot density not including pore space which we assume to be occupied by the solution) is assumed constant. Eqs. 6.10-6.14 when used in eq. 6.9 constitute a thermodynamic prediction of the aerodynamic diameter ratio. We show the expected qualitative growth on sulfuric acid coated soot in fig. 6-3.

The implication of eq. 6.9 is that (in the case where the sulfuric mass is much greater than the soot mass within the particle) we can model a size distribution of such aerosols at a relative humidity, RH by simply translating the distribution present at RH_0 by a constant multiplicative factor. This is illustrated with actual experimental data in fig. 6-4.

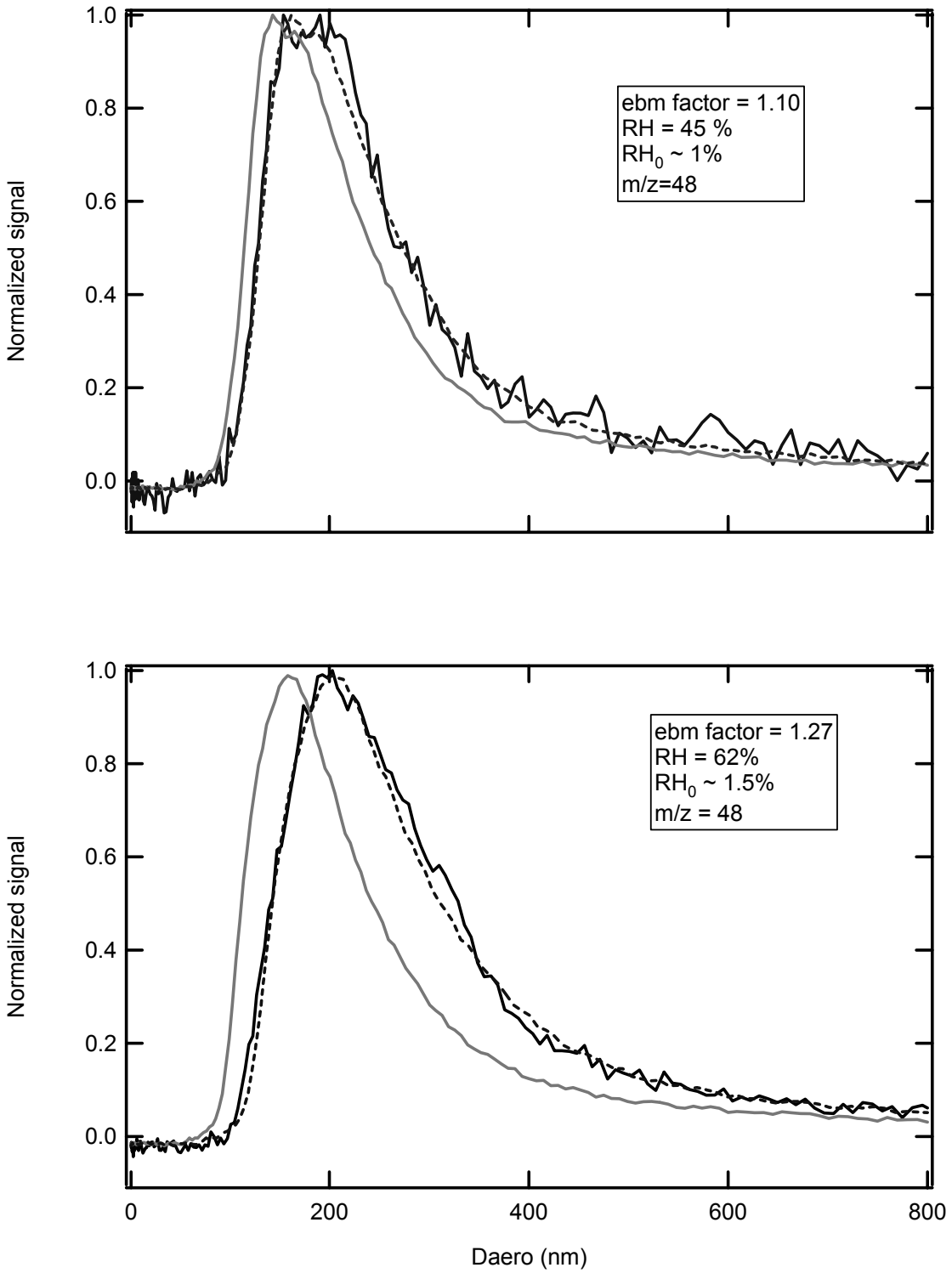

Figure 6-4: Growth on sulfuric acid at two different relative humidities. The dashed line is constructed by translating the gray line rightward by a multiplicative equilibrium (ebm) factor (see eq. 6.9)

In fig. 6-4 the distribution at high RH is reproduced by a horizontal projection of the distribution at the initial RH. This is achieved by multiplying each initial "dry" aerodynamic diameter by a single constant, representing the fractional growth experienced by each particle. This demonstrates that water adds "bulk-wise" into the particles; more is added to larger particles. This is in contrast to a simple addition of a layer of a certain thickness. This observation is consistent with the equilibrium model of water uptake described in eq. 6.9.

6.2 Coagulation of sulfuric acid aerosols

Here we present aspects of aerosol microphysics from the perspective of experiments involving sulfuric acid aerosol formation, growth, and coagulation. Nucleation and growth aspects are presented in order to develop an understanding of the experimental conditions enabling a quantitative investigation of aerosol coagulation. Presenting the microphysics in such a comprehensive fashion, we hope to inspire future studies requiring bolder experimental and modeling efforts than we presently undertake. Indeed, experimental and numerical modeling techniques have made such strides in recent years that the sort of dynamic complexity associated with such systems is no longer beyond meaningful quantitative investigation[3]. While the results of the study presented here are only preliminary in nature, they enable us to outline a methodology for obtaining quantitative information on coagulating aerosol systems.

In general, particle formation, growth, and coagulation are highly coupled processes for which the coupled dynamics can only be described by the general

dynamic equation (GDE). We will instead present each process separately, developing the required mathematics as we go, but general numerical solutions of the GDE (presently an active research area) will be required for thorough investigations of such systems over the full range of conditions encountered in the atmosphere. In addition, this individual treatment of nucleation, condensation, and coagulation will enable us to develop the experimental method that successfully separates coagulation from the other two processes.

6.2.1 Outline of experimental method

A sulfuric acid reservoir heated to a known temperature is connected to a flowtube via heated tubing. Dry filtered nitrogen carrier gas is pre-heated and passed over the reservoir entraining gas phase H_2SO_4 to the flowtube. The entrance to the flowtube is heated to a temperature above that of the reservoir, establishing a well-characterized decreasing temperature profile along the flowtube axis. Supersaturation (and consequent nucleation and growth) conditions are reached at a position within the flowtube determined by the temperature profile and the H_2SO_4 vapor pressure (see sec. 7.1).

The apparatus is shown in fig. 6-5. In our preliminary experiments, nitrogen gas heated to a temperature slightly higher than that of the sulfuric acid reservoir (T_{res}) was flowed over the reservoir at 900 cc min^{-1}. A fraction of the equilibrium concentration of gas phase sulfuric acid in the reservoir was entrained into a 1.092 cm radius flowtube for which the entrance temperature is fixed at 150 C ($>T_{res}$). The flow here is laminar (Re ~ 100) at one atmosphere total pressure, with an axial flow

speed of ~ 8 cm s^{-1}. Nearing the AMS inlet, the temperature within an axial air parcel decreases with a well-established profile, leading to supersaturations, $S > 1$ in less than ~1 second (fig. 6-6). The combined effect of decreasing temperature and increasing supersaturation leads to a very steep increase in the homogeneous nucleation rate (fig. 6-7**,** and sec. 7.1). The very rapid formation of critical cluster nuclei and consequent condensational growth on each nuclei leads to a very rapid decrease in *S*. This establishes a nucleation / condensation burst with a duration of ~ 0.3 s (fig. 6-7 and sec. 7.2). The particles nascent in the system at this time constitute the initial number density of size-1 particles at density n_0 and size D_0. Typical calculated burst times are near 1.5 s from the flowtube entrance, such that the total coagulation time, t_c is 4.5(+/-0.2) s for T_{res} ranging from 74 to 101 C.

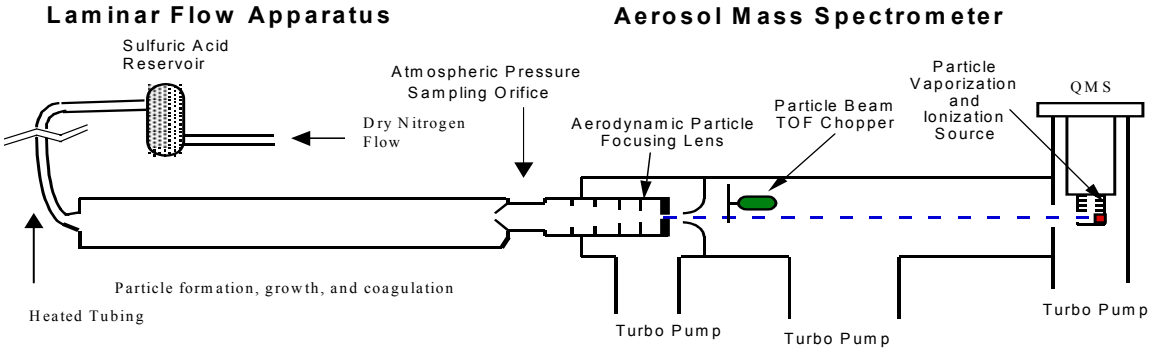

Figure 6-5: Experimental apparatus using AMS detection of evolving aerosol size and mass distributions in a laminar flowtube.

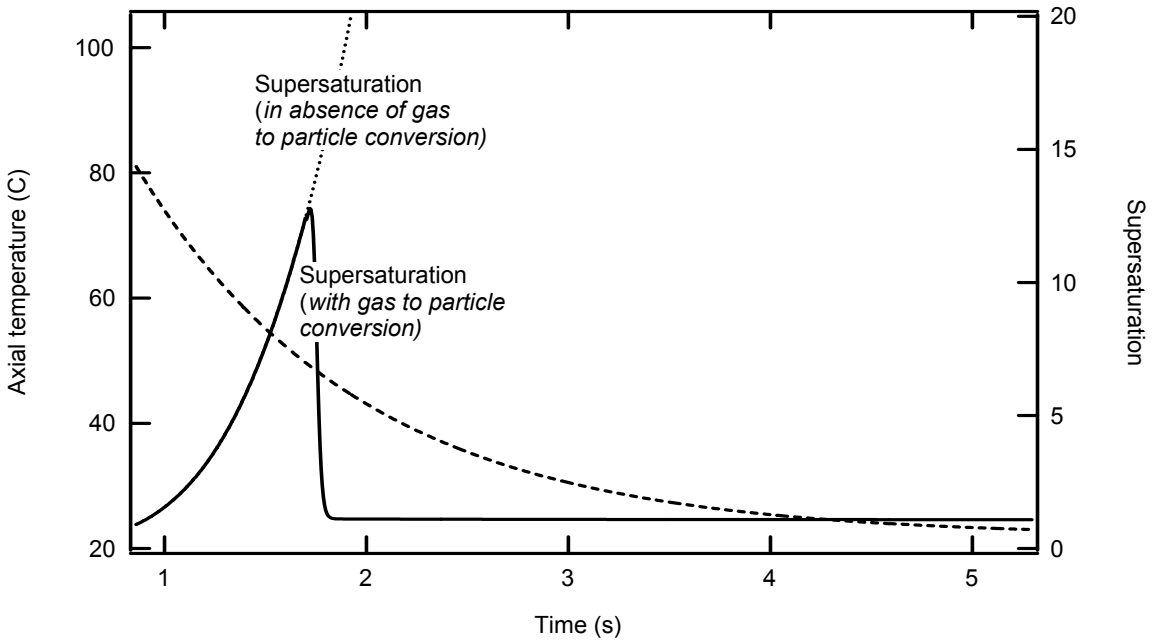

Figure 6-6: In the presence of gas to particle conversions, the supersaturation spikes at near 1.5 seconds. Very rapid condensation on particles sustains $S = 1$ for the remaining duration of the flow time.

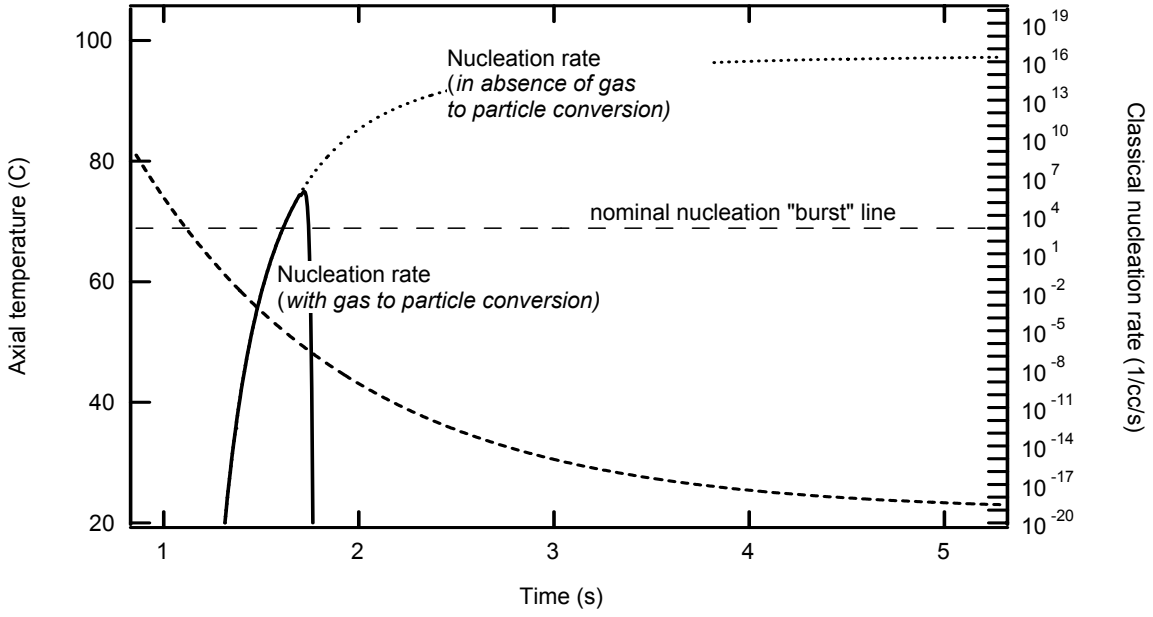

Figure 6-7: In the presence of gas to particle conversions, the nucleation rate spikes at around 1.5 s in the flowtube.

By matching the flow speeds (~ 8 cm/s) of the carrier gas and the inlet flow speed into the AMS, the resulting coagulated aerosols can be isokinetically sampled into the instrument (at 1.5 cc s^{-1}) through the 120 μm orifice opening. Isokinetic conditions are necessary for accurate determination of particle coagulation times. We note that due to the small diffusion coefficient of submicron aerosols at 1 atm (D ~10^{-5} cm^2 s^{-1}), the aerosol loss rate to the walls is negligible. Also, gas phase losses to the walls occur with a characteristic time of ~ R^2/D_g = $1.092^2/0.1$ ~ 12 s, so they are not significant over the particle formation time (~0.5 s).

6.2.2 A simple model of coagulation kinetics

Here we formulate a model of the coagulation kinetics of five different sizes. From the possible collisions we have:

$$\begin{aligned} M + M &\xrightarrow{k_{11}} D \\ M + D &\xrightarrow{k_{12}} T \\ M + T &\xrightarrow{k_{13}} Q \\ M + Q &\xrightarrow{k_{14}} P \\ D + D &\xrightarrow{k_{22}} Q \\ D + T &\xrightarrow{k_{23}} P \end{aligned} \qquad (6.15)$$

As written the k_{ij} can also be thought of as formation rate constants, since for every collision there is formation of one (i+j)-mer. Here M represents the *monomer* (size-1), D represents the *dimer* resulting from an *M:M* collision, T represents the *trimer* resulting from an *M:D* collision, Q represents the *4-mer* resulting from either an *M:T* or a *D:D* collision and P represents the *5-mer* resulting from an *M:Q* or *D:T* collision. This leads to the following system of differential equations:

$$\begin{aligned}
\dot{n}_1 &= -2k_{11}{n_1}^2 - k_{12}n_1n_2 - k_{13}n_1n_3 - k_{14}n_1n_4 \\
\dot{n}_2 &= k_{11}{n_1}^2 - k_{12}n_1n_2 - 2k_{22}{n_2}^2 - k_{23}n_2n_3 \\
\dot{n}_3 &= k_{12}n_1n_2 - k_{13}n_1n_3 - k_{23}n_2n_3 \\
\dot{n}_4 &= k_{13}n_1n_3 - k_{14}n_1n_4 + k_{22}{n_2}^2 \\
\dot{n}_5 &= k_{14}n_1n_4 + k_{23}n_2n_3
\end{aligned} \tag{6.16}$$

The concept is illustrated schematically in fig. 6-8. This system, taken with the initial conditions, $n_1(0) = n_0$, $n_i(0) = 0$ (for i=2,3,4,5), and $t_c = 4.5$ s, defines the $n_i(t_c)$ for each constant k_{ij}. This model has been validated to test the limitations of some of its underlying assumptions (sec. 7.3).

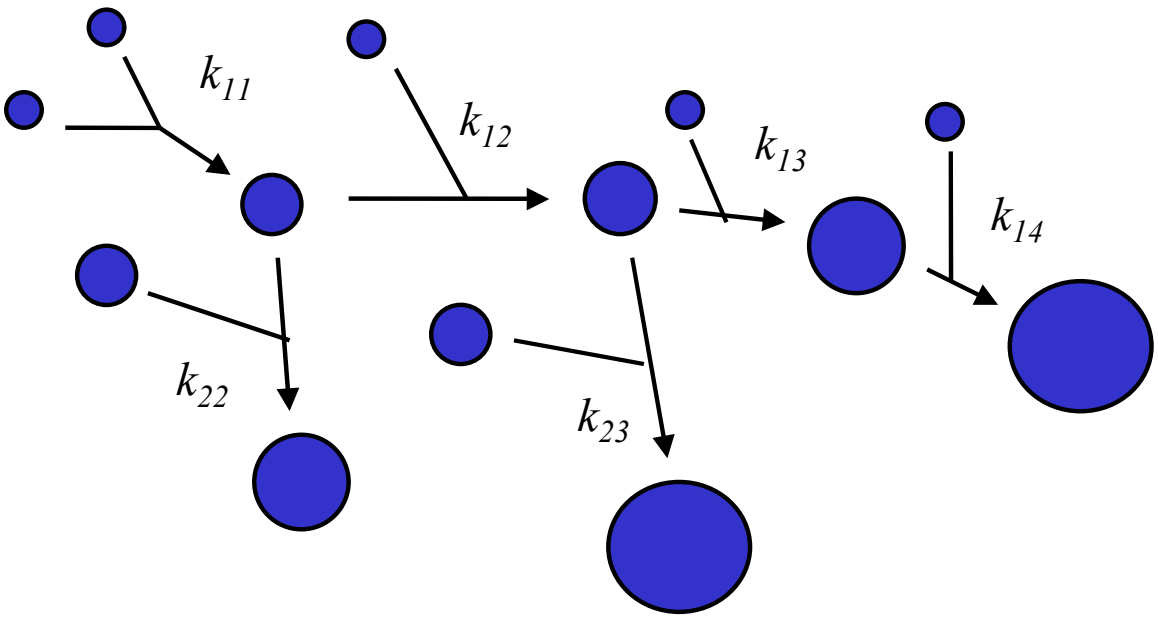

Figure 6-8: Coagulation of particles of multiple sizes.

6.2.3 Outline of data analysis

The AMS samples particles formed in the flowtube where their mass distributions are measured. In this experimental example, particle coagulation was observed over the range of initial particle number densities, 3.9 x 10^7 to 1.1 x 10^8 cc^{-1}. As described above (sec. 3.4.2), a sum of lognormal size distributions can be fit to the calibrated raw AMS mass distributions providing information on the number of particles within a given size mode. From such fits to the raw data, we obtain lognormal distribution parameters (n_i, D_i, and σ_i) describing the aerosol ensembles at each reservoir temperature, T_{res}. The mode number densities, n_i taken from the fits are then linked to the initial number density, n_0 based on mass conservation (see sec. 7.4): $n_0 = \Sigma i n_i$. We then plot the n_i as a function of n_0 to obtain a model fit. It may be argued that there is some circularity in this approach as the n_i appear already in the calculated n_0. However, while it is true that n_0 is defined by the n_i, each n_i is not defined by n_0. Put another way, there are very many ways to add the n_i and recover n_0. The detailed kinetics fixes one such way.

6.2.4 System mass conservation

Fig. 6-9 illustrates the overall mass conservation in the flowtube by comparing the particle mass loading to the calculated gas mass loading at equilibrium in the reservoir. The saturation extent is nearly constant over an order of magnitude change in gas mass. Since we know both the total mass in the flowtube and the initial number of size 1 particles, we may calculate their initial diameter through mass conservation: $n_0 \rho \pi D_0^3/6 = M_0$. The result shows D_0 to be within about 10% of D_1 as obtained from the

fit. This result attests to the overall consistency of the results, including: constant extent of saturation in the flowtube, accurate calculation of n_0, the lens transmission function used to correct the fits, and the absence of gas phase wall losses.

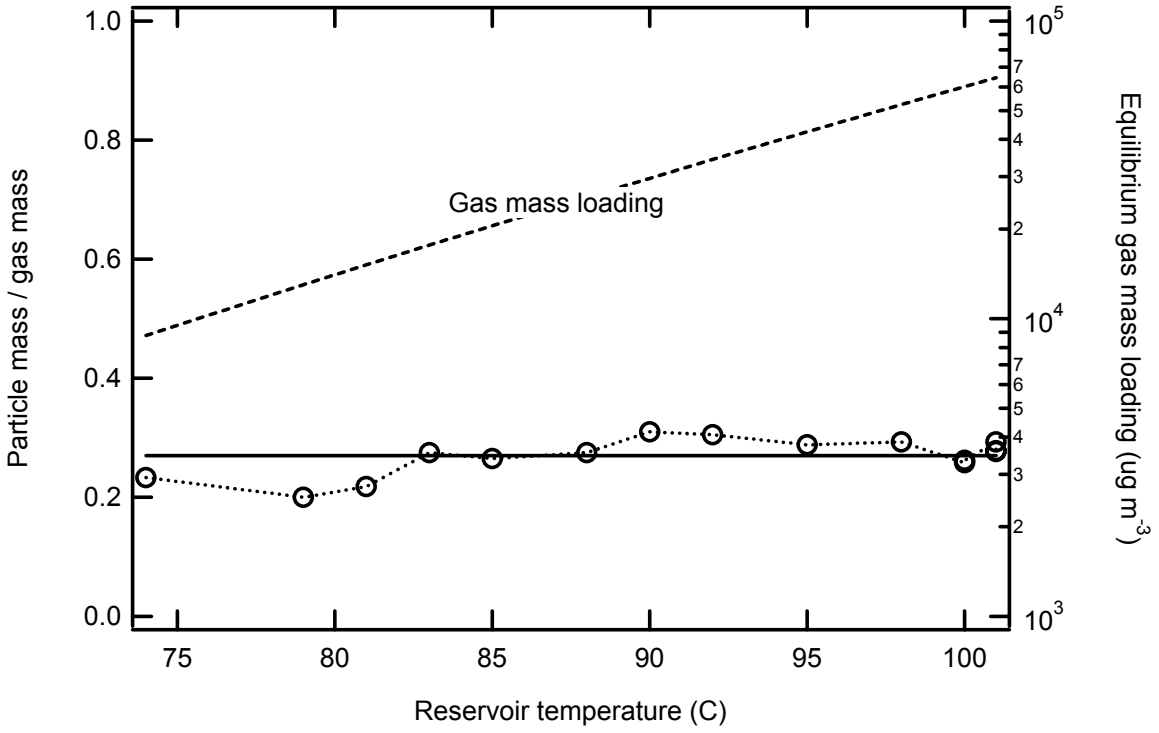

Figure 6-9: The saturation extent is constant at ~ 0.25 over an order of magnitude change in gas mass loading in the reservoir.

Chapter 6 References

[1] Report of the International Panel on Climate Change, 1995.

[2] News feature, *Nature,* **407**,10-12, (2000).

[3] D. D. Obrigkeit, *Numerical Solutions of Multicomponent Population Balance Systems with Applications to Particulate Processes*, PhD Thesis, MIT, 2001.